Bode plots applied to microscopic interferometry

J.M. Flores, M. Cywiak*, M. Servín, and L. Juárez
Centro de Investigaciones en Óptica, A.C.,
Loma del Bosque 115, Lomas del Campestre, León, Guanajuato, 37150 México,
*e-mail: moi@cio.mx

We describe a technique for using Bode plots in microscopic interferometry, in particular as applied to the three Gaussian beam interferometer recently reported in the literature. The technique is used in a similar manner to its application to an electric or electronic system in finding its frequency response. The Bode response is used to deconvolve the raw data obtained directly from the interferometer to compensate for the data in frequency, making it possible to obtain more realistic profiles of the samples under test. We apply this technique to obtain profiles of the inner reflective layers of two optical types of surfaces for data storage commercially available, namely, the compact disk (CD-R) and the digital versatile disk (DVD-R). We report the experimental results of radial scans of these devices without data marks, before and after applying the transfer function of the system. The measurements are obtained by placing the devices with the polycarbonate surfaces so as to aim the probe beam of the interferometer at them, taking advantage of the vertical depth discrimination of the microscope. We show that the resulting profiles, obtained across the Polycarbonate layer, measured with this interferometer, give valuable information of the real track profiles, making the combination of the Bode plots with this interferometer a suitable tool for quality control of the surface storage devices.

Keywords: Bode transform; gaussian beam; interferometry.

Describimos una técnica que permite utilizar las gráficas de Bode en interferometría microscópica, en particular aplicada al interferómetro de tres haces Gaussianos recientemente reportado en la literatura. La técnica es utilizada de una manera similar a la forma en que se hace para encontrar la respuesta en frecuencia de un sistema eléctrico o electrónico. La respuesta de Bode es utilizada para calcular la deconvolución de los datos crudos obtenidos directamente del interferómetro para compensar los datos en frecuencia, permitiendo obtener un perfil más realista de las muestras bajo prueba. Aplicamos la técnica para obtener los perfiles de las superficies reflectoras internas de dos dispositivos ópticos comercialmente disponibles para almacenamiento de datos, el disco compacto (CD-R) y el disco digital versátil (DVD-R). Reportamos resultados experimentales de una exploración radial de estos dispositivos sin datos almacenados, antes y después de aplicar la función de transferencia del sistema. Las mediciones son obtenidas colocando los dispositivos con la superficie de Policarbonato apuntando al haz de prueba del interferómetro, aprovechando la ventaja de la discriminación de profundidad del microscopio. Mostramos que los perfiles resultantes, obtenidos a través de la capa del Policarbonato, medidos con este interferómetro, proporcionan información valiosa de los perfiles reales de las pistas de estos dispositivos, por lo que la combinación de Bode aunada al uso de este interferómetro representan una herramienta adecuada para el control de calidad de los dispositivos ópticos de almacenamiento de datos mencionados.

Descriptores: Bode transform; gaussian beam; interferometry.

PACS: 07.60.; 42.79.Vb; 42.87._d

1. Introduction

Bode plots represent a useful tool for determining and analyzing the frequency response of an electronic or electrical system. These plots make it possible to detect important properties of the response of a system, for example, resonance frequencies. Two types of Bode plots are commonly used, namely magnitude vs. frequency, and phase vs. frequency. In this report, we are interested in the first plot.

Bode plots are based on the poles and zeros of a system and are commonly used in feedback theory. In addition, the shape of the frequency response of the system makes it possible to compensate for the resulting outputs by means of a deconvolution process. The magnitude versus frequency response is called the transfer function of the system and it is obtained simply by finding many frequency values, calculating the magnitude of the output at each frequency and charting them against a frequency coordinate.

It can be said in summary, as described in Refs. 1 and 2, that Bode plots represent two main aspects:

- They compress the spectral information of the function along the spectral axis. This permits the measurement of the dangerous (undamped) frequencies of a given system *i.e.*, the poles of the frequency response function.

- The above information of the dangerous frequencies is important for anticipating the noise and stability performance of the system.

For applying the Bode method to an optical system, in this report, we have chosen the three-Gaussian beam interferometer (TGBI) [3]. We have selected this interferometer because it exhibits a Gaussian transfer function, centered at the origin, thus making it simple to perform the process of deconvolution. We present the methodology for finding the Bode plots for the TGBI by measuring several reflecting gratings with different pitches, commercially available. The technique presented here is intended to be used in any interferometric microscope by using a set of calibrated gratings, in analogy with the sweep generator used in electronics.

The presentation of this report is as follows. In the next section we describe the TGBI, which consists on of the heterodyning of three beams with a Gaussian intensity profile. In sub-Sec. 2.1 our proposal to obtain the Bode response is described and then applied for measuring the profiles of two optical storage devices, a CD and a DVD without data marks. In Sec. 3, we present the experimental results of the measurements of the profiles of the optical devices. Finally, our conclusions are presented in Sec. 4.

2. The three Gaussian beam interferometer

Figure 1 depicts the experimental setup that corresponds to the three Gaussian beam interferometer [3]. A He-Ne laser with a Gaussian intensity profile is used as the coherent illuminating source. The illuminating beam is transmitted through a Bragg cell that consists of an acousto-optical medium of tellurium dioxide (TeO$_2$) excited at 80 Mhz. Only the diffracted orders zero and one are used, and all other orders are blocked. The order zero is directed to beam splitter BS1, where it is split into two beams. One of them, the probe beam, is focused on the surface under test by lens L1. After being reflected, the probe beam is modulated in its phase by the local surface irregularities, transmitted again by lens L1 and directed to the photo-detector by means of BS1. The second beam, the reference beam, after being reflected from a high quality reference surface, M3, is directed to the photo-detector also by means of BS1. Finally, the order one diffracted at the output of the Bragg cell is guided towards the photo-detector by means of mirrors M1 and M2 and by beam splitter BS2. The temporal frequency of this beam corresponds to the sum of the temporal frequency of the illuminating source and the frequency of excitation of the acousto-optical cell; this beam will be referred to as the modulating beam. As depicted, the three beams are superimposed and coherently added at the sensitive plane of the photo-detector.
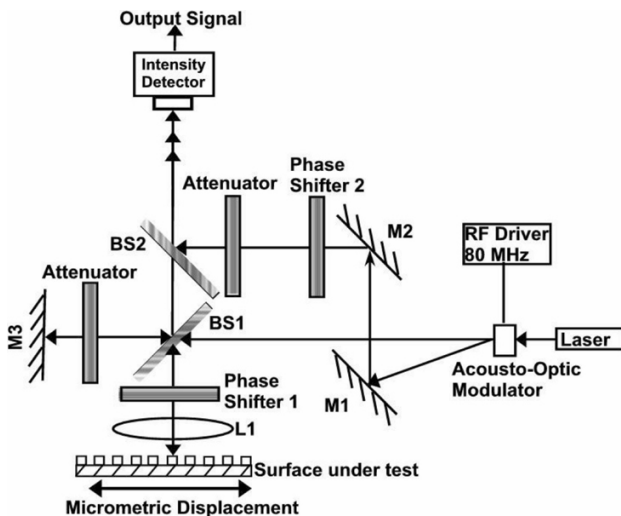

FIGURE 1. Experimental set up.

The photo-detector is chosen to be large enough so as to integrate the overall intensity of the beams. The signal at its output is amplified and sent to a lock-in amplifier for A.C. detection and recording.

Two phase-shifters PS1 and PS2 are used, introducing a phase shift of $\pi/2$ and $\pi\, rad$ respectively. When the phase shifters are properly adjusted, the output signal results in a sine function whose argument is proportional to the local vertical height under measurement, as shown analytically in Ref. 3, giving the system high vertical sensitivity. The use of both attenuators depicted in the diagram is optional and their use is only to simplify the analytical formulation, by equalizing the three intensities at the plane of the photodiode.

Let $\Psi_0 (x, y)$ be the amplitude distribution of the Gaussian beam focused at the surface under test,

$$\Psi_0 (x, y) = \left(\frac{2P_0}{\pi\, r_0^2} \right)^{\frac{1}{2}} \exp \left[-\frac{(x-x_0)^2 + (y-y_0)^2}{r_0^2} \right], \quad (1)$$

where, P_0 is the beam power, r_0 is the semi-width and (x_0, y_0) are the coordinates of the beam center.

A mathematical analysis can be found in Ref. 3, where a step-by-step deduction of the equations that govern the operation of the interferometer is presented. As indicated in Ref. 3, the sensitive area of the photodetector is large enough to integrate the overall intensity distribution of the incoming beams; thus at the output of the intensity detector, a trans-impedance amplifier will give a DC signal plus an AC signal. As a lock-in amplifier is used for narrow-band detection, only the time varying voltage signal, tuned at 80 Mhz is detected, filtering out undesirable noise. The amplitude of the output signal is given as,

$$V(x_0, y_0) = \frac{4P_0}{\pi\, r_0^2} A\rho$$

$$\times \int_{-\infty}^{+\infty} \int_{-\infty}^{+\infty} \exp \left[-\frac{2 \left[(x - x_0)^2 + (y - y_0)^2 \right]}{r_0^2} \right]$$

$$\times \sin \left[\frac{2\pi}{\lambda} h(x, y) \right] dx dy. \quad (2)$$

The function $h(x, y)$ represents the height amplitude distribution of the surface under test, A is the gain of the amplifier, ρ the photodiode responsivity, and λ is the wavelength of the illuminating source.

Equation (2) can be described as follows. Let

$$\sin \left[\frac{2\pi}{\lambda} h(x, y) \right] \cong \frac{2\pi}{\lambda} h(x, y)$$

for small $h(x, y)$; then Eq. (2) will indicate a convolution of a Gaussian function with the amplitude distribution of the surface under test. Thus, this Gaussian function represents the impulse response of the system. As is well known, the Fourier transform of a Gaussian is also a Gaussian. Thus, the transfer function of the system is a Gaussian centered function.

2.1. Determination of the frequency system response and calibration procedure

As can be seen from Eq. (2), the whole optical process can be represented as the convolution of the system impulse response with the sine of the input function. The impulse response is then,

$$\mathrm{K}(x_0, y_0) = \exp\left[\frac{-2\left(x_0^2 + y_0^2\right)}{r_0^2}\right]. \tag{3}$$

Using Eq. (3), it allows us to write Eq. (2) as

$$V(x_0, y_0) = \frac{4P_0}{\pi \, r_0^2} A\rho$$

$$\times \int\limits_{-\infty}^{+\infty} \int\limits_{-\infty}^{+\infty} \mathrm{K}(x - x_0, y - y_0)$$

$$\times \sin\left[\frac{2\pi}{\lambda} h(x, y)\right] \, dx \, dy. \tag{4}$$

Equation (4) indicates that to obtain the local surface height, $h(x_0, y_0)$, a deconvolution process has to be performed and an inverse sine has to be calculated. However, as the object of this manuscript is limited in showing the principle of the technique, we shall follow a simpler approach, which gives accurate results for the measurements of interest in this report. One of the measurements consists in obtaining the topography of three holographic reflecting gratings whose pitches are 300, 600 and 1200 lines/mm; the vertical height of the gratings being less than $\lambda/4$. The measurement of the grating topographies will serve to obtain the Bode plot of the interferometer.

For the samples just described, studied in the experimental part of this work, Eq. (2) can be approximated as

$$V(x_0, y_0) = \frac{4P_0}{\pi \, r_0^2} A\rho \, \sin\left[\frac{2\pi}{\lambda} h(x_0, y_0)\right]. \tag{5}$$

Equation (5) has been introduced only for descriptive purposes and can be considered a first order approximation. This can be confirmed by computer simulations, calculating the convolution of the impulse Gaussian function with semi-width r_0=0.44 μm, with the three gratings described. In Sec. 3, profiles that are more realistic will be obtained by calculating the convolution indicated by Eq. (4).

From Eq. (5) one obtains the local height at (x_0, y_0) as

$$h(x_0, y_0) = \frac{\lambda}{2\pi} \sin^{-1}\left[\frac{\pi \, r_0^2 V(x_0, y_0)}{4A\rho P_0}\right]. \tag{6}$$

In addition, we notice that for heights less than $\lambda/4$, phase unwrapping techniques are not necessary. However, in general an unwrapping technique may be required. As indicated above, Eqs. (5) and (6) are introduced only for illustrative purposes.

It should be remarked that the interferometer works with Gaussian beams. The focusing lens has an aperture large enough to transmit the beams (forward and reflected), without any clipping. Thus, the Fresnel diffraction integral can be used to calculate the overall propagation of the beams, in particular the semi-width of the focusing spot. Let R_0 be the semi-width at the output of the He-Ne laser ($\cong 0.72$ mm in our case). For an easy placement of the components in the experimental set-up, the distance from the laser output to the focusing lens was chosen of approximately 2 m. Thus, with a focal length of 2 mm one obtains for the Gaussian beam focused at the surface under test a semi-width $r_0 = 0.44$ μm. The corresponding focusing distance is at 2.001 mm. Thus, the distance where the probe beam is best focussed is located slightly away from the focal distance of the lens. Experimentally, placement of the surface under test at this position can easily be achieved by monitoring the reflected light.

As mentioned above, to obtain the Bode plot of the system, three holographic reflecting gratings with pitches 300, 600 and 1200 lines/mm were measured and compared with the results of an AFM (Atomic Force Microscope). It should be pointed out that more gratings are required for better accuracy; however, taking advantage of our a-priori knowledge of the Gaussian transfer function, for this report, we shall limit ourselves to showing the principle of the technique. For obtaining a Bode plot with accuracy for a general microscope interferometer, a set of several gratings will be necessary.

To obtain the Bode plot of the system, it is necessary to calculate the Fourier transform of the impulse response of the system. Taking the Fourier transform of Eq. (3) as

$$\Im\{\mathrm{K}(x_0, y_0)\} = \int\limits_{-\infty}^{+\infty} \int\limits_{-\infty}^{+\infty} \exp\left[\frac{-2\left(x_0^2 + y_0^2\right)}{r_0^2}\right]$$

$$\times \exp\left[-i2\pi\left(ux_0 + vy_0\right)\right] dx_0 dy_0, \tag{7}$$

it allows us to express the transfer function of the system as

$$F(u, v) = \frac{\pi \, r_0^2}{2} \exp\left(-\pi^2 r_0^2 \frac{u^2 + v^2}{2}\right). \tag{8}$$

From Eq. (8) the cut-off frequency of the system (in one dimension) is

$$u_C = \frac{\sqrt{2}}{\pi \, r_0}. \tag{9}$$

As $r_0 = 0.44$ μm, the cut-off frequency

$$u_c = 1.023 \times 10^6 m^{-1}.$$

Thus, formally, for an object under test consisting of a grating, the shortest period that this system would detect is about 0.98 μm.

The physical reason for the limitation in the lateral resolution depends on capturing the diffracted orders reflected from the surface under test. With lens L1 being a microscope lens having a numerical aperture of 0.7, mainly the first orders diffracted by the reflecting grating are captured for detection.

Thus, subsurface features are difficult to detect. This problem can be alleviated by using an illuminating beam having a shorter wavelength and also by using a lens with a larger numerical aperture.

The frequency response represented by Eq. (8) is a consequence of the Gaussian intensity profile of the probe beam. Several measurements were taken for each of the gratings in a small zone of interest and compared with the results of the

AFM. The AFM, gives the results in real height (nm) and the proposed system in Volts, according to Eq. (6). For the proposed system, the calibration technique is as follows.

First, for each grating an average height distribution over the small zone of interest was estimated. The three averages (one for each grating), obtained with the AFM, are shown in Fig. 2a (Right). For each of these three average distributions, an rms vertical height value was obtained for each grating.
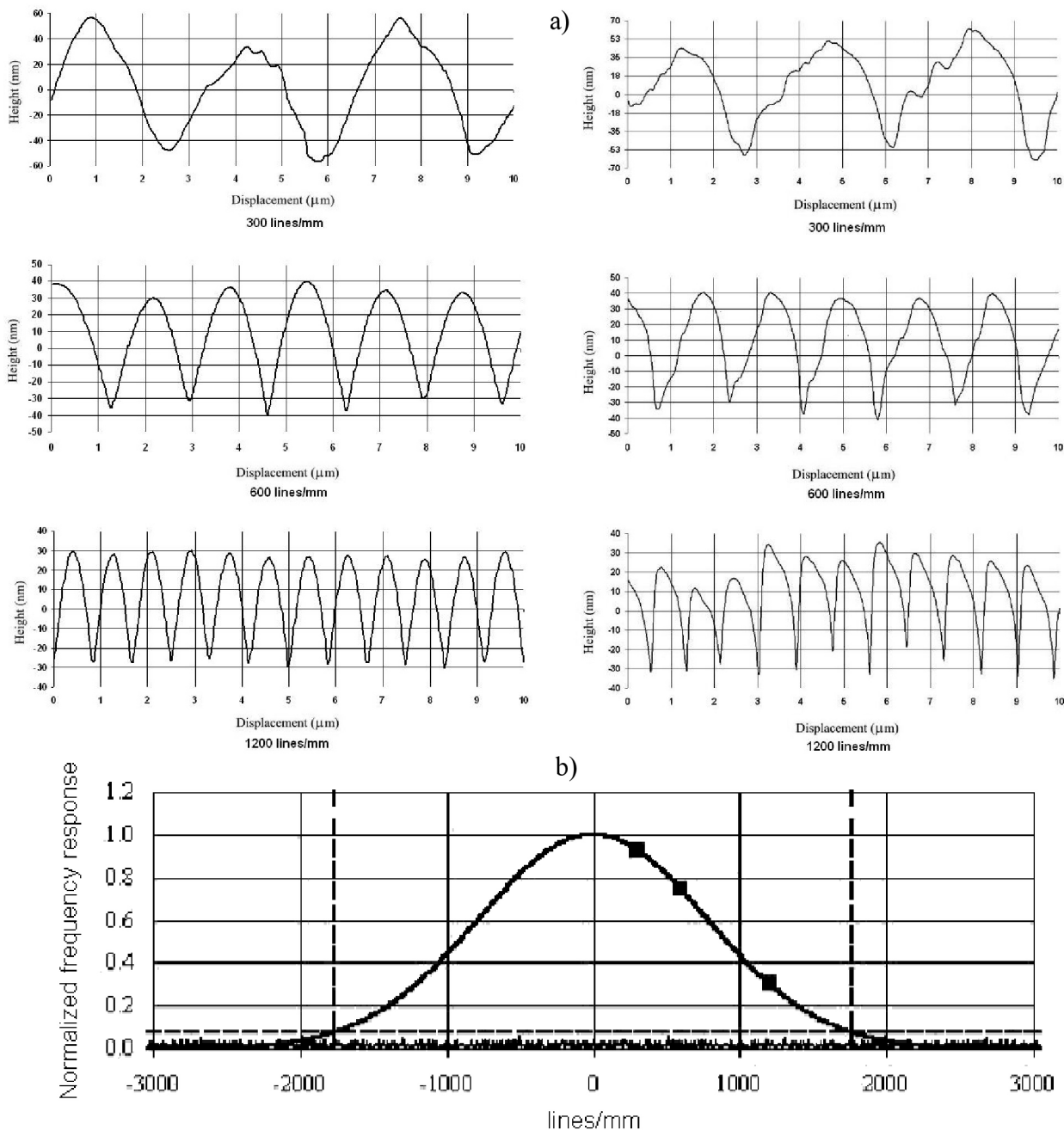

FIGURE 2. a). (Left) Line-profiles obtained with the interferometric technique. (Right) Line-profiles obtained with an atomic force microscope. b). Plot of the normalized frequency response of the system and the corresponding noise distribution.

Second, for each grating an average height distribution was obtained with the proposed technique, however, this time, the resulting height distributions were obtained in volts as expressed by Eq. (2). These measurements are shown on the left side of Fig. 2a, already in nanometers as described bellow.

In order to convert the Volts obtained for each grating into nanomemeters, we took in consideration the following parameters:

i) the responsivity (ρ) of the photodetector, given in Amperes/Watt

ii) the gain of the trans-impedance amplifier at the output of the photodetector, and

iii) the power of the beam focused on the sample, which can be written as $P_0 = A_d I_0$, where A_d is the area of the photodiode and I_0 the intensity of the beam, according to Eq. (6). Thus, we obtain directly the height of the surface under test from the voltage measured by the photodetector. This information is sent to a Lock-in amplifier and processed by a computer. The scanning distance is obtained by means of a previously calibrated flexured piezoelectric (PZT).

Before proceeding with the experimental description, a discussion on the results depicted in Fig. 2a is given. A direct, detailed comparison between methods is not simple, as it is not possible to achieve exactly the same line scan with both methods. In addition, the optical system is limited in its lateral resolution because of diffraction; as usual, one can consider λg to be a limit. Further, the AFM responds to different physical properties as compared with the optical system. An ample discussion on this topic can be found in Ref. 22. Figure 2a (Left) reveals that, the more difficult case, the grating with a spatial frequency of 1200 lines/mm ($period = 0.83$ μm), can easily be detected with the proposed method. Thus a lateral resolution near λg is attained. This is attributed to the high vertical sensitivity of the system that in turn improves the lateral resolution. Thus, for a reasonable comparison of the methods, the average rms values of a set of measurements are used.

Third, from the above rms values obtained, the ratios of the rms output voltages to the rms corresponding heights were calculated for each spatial frequency.

A frequency response curve for the above ratios was fitted. For simplicity, a normalized plot is shown in Fig. 2b. It will be noticed that the frequency response experimentally obtained is in good agreement with the theoretical response given by Eq. (9).

As previously mentioned, the curve of the response was adjusted by using only three points. This is done only for illustrative purposes and more points can be added if desired. For clarity, a symmetric spatial frequency axis is shown.
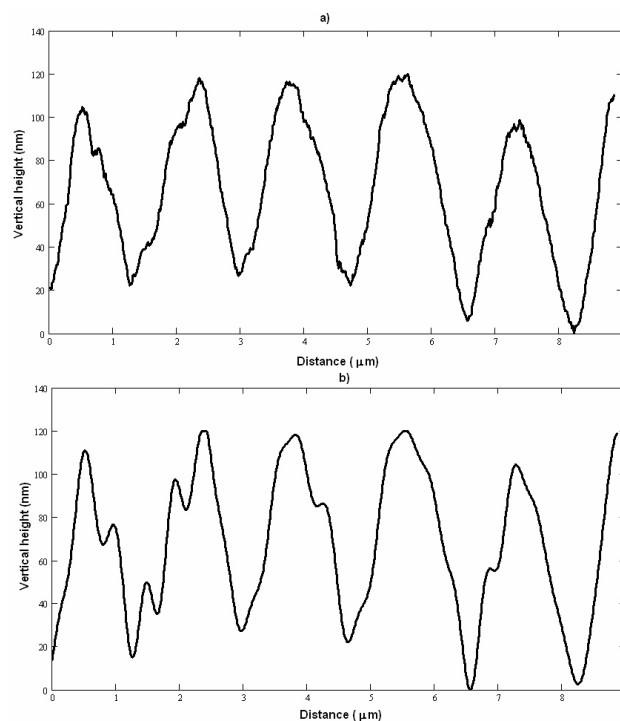

FIGURE 3. Line scans of a) CD-R and b) CD-R after the deconvolution process.
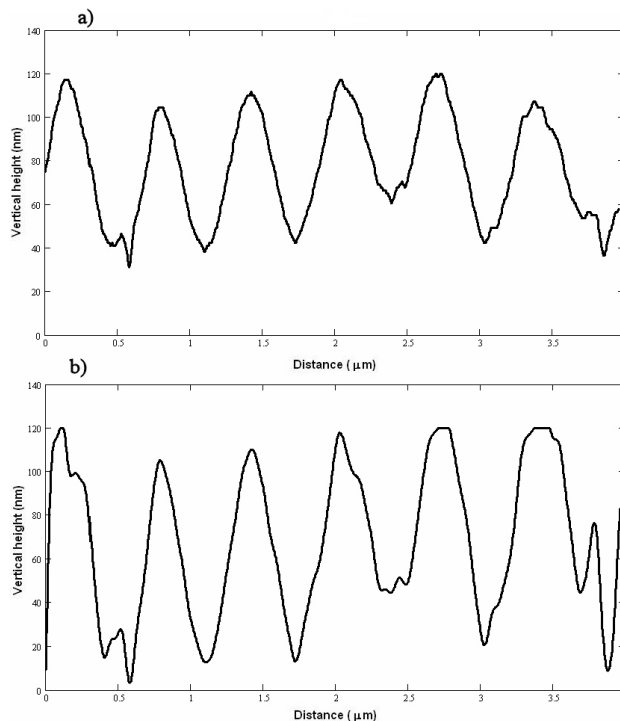

FIGURE 4. Line scans of a) DVD-R and b) DVD-R after the deconvolution process.

Figure 2b also shows the noise distribution on a scale that corresponds to the normalized frequency response, and was obtained as follows. The average profile obtained for each of the gratings was subtracted from each of the measurements.

Then, by placing each result of each subtraction one after another, a set was formed. This gives a representative noise of the set of samples. Finally, the Fourier transform of the set was obtained and plotted. In Fig. 2b the vertical dotted lines indicate the useful area inside the filter that can be used to recover the input profile to be measured by the system.

3.   Profile measurements

For the experiments, we arbitrarily chose a Sony® CD-R and a Verbatim® DVD-R without data marks. The probe beam enters at a normal incidence, propagating across the Polycarbonate layer, and travels back after being reflected by the reflective surface, taking advantage of the vertical depth discrimination of the (TGBI). Other techniques require special preparation for the measurements (see for example Refs. 5 to 16). In addition, in the manufacture processing, it is common to use an atomic force microscope (AFM) [17-21] before the Polycarbonate layer is deposited.

It is important to mention that the CD and DVD reflecting surfaces being measured, can be considered reflecting gratings with periods 1.6 and 0.74 μm respectively. As the lateral dimensions of the tracks are different between the CD and the DVD, to attain a similar visualization of a certain number of tracks for the CD-R, a line scan of approximately 10 μm was performed and for the DVD-R, a line scan of 5 μm was chosen. In each scan, 1500 sample points were recorded. Figure 3 shows the resulting profiles of the CD-R before and after the deconvolution process. Figure 4 shows the experimental profiles for the DVD before and after the deconvolution process. After processing, a more realistic profile is expected as the high frequency features recover their original amplitude value. This would not be possible if one used Eqs. (5) directly. and (6). In adddition, the deconvolution was performed inside the valid frequency of the filter; thus, an additional advantage is that some noise has been filtered out as can be appreciated in the reported results.

The measurements shown are in good agreement with the lateral width of the tracks, measured with other techniques extensively reported, as for example Refs. 5 to 21. As indicated above, these techniques include the atomic force microscope (AFM), the scanning probe microscope (SPM), the reflection-mode scattering-type scanning near-field optical microscope (RS-SNOM), the conductive-atomic force microscope (C-AFM), the transmission electron microscope (TEM) and the scanning electron microscope (SEM). As

mentioned, the advantage of the TGBI, being a far field technique, is its capability to measure the tracks across the Polycarbonate layer, as indicated above. This is due to the high vertical depth of field discrimination which is typical of scanning systems that use focused probe beams.

Before finishing this report, we would like to mention that nowadays it is of great interest, to measure the profiles of new high-density devices, as is the case of the blue ray. These measurements can easily be performed with the TGBI, which only requires replacing the illuminating source beam with a smaller wavelength. However, for the time being, we are not in a position to perform this experimental test.

4.   Conclusions

We have shown that Bode plots can be used to obtain more realistic information about the surface under measurement by deconvolving the raw data obtained directly from an optical inteferometric microscope. We have applied the technique for profiling the reflected surfaces inside two different commercially available "optical data storage devices" corresponding to a CD-R and DVD-R, by using the three - Gaussian- beam interferometer. Normalized measurements of the tracks in a radial scan of micrometric length were shown. These measurements were taken across the Polycarbonate layer that covers the optical disks. The resulting profiles showed high lateral and vertical resolution, with low noise. The feasibility of applying Bode plots was shown by choosing a particular optical interferometric system characterized by a Gaussian centered transfer function. The technique can be generalized to any arbitrary microscopic interferometer. By applying the curve of the frequency response to the raw experimental data, a profile that better resembles the real surface was obtained. A collateral conclusion is that the combination of the three -Gaussian- beam interferometer with the deconvolution with the transfer function calculated by the Bode plot turns out to be appropriate for quality inspection in the production of optical data storage devices. The same technique can be applied to profile the new high-density devices just by reducing the wavelength of the illuminating source.

Acknowledgments

1. H.W. Bode, "*Network Analysis and Feedback Amplifier Design*" (Van Nostrand, Princeton, N.J., 1945) Chap.13, p.286; Chap.15, p.337.

2. Z. Zalevsky and D. Mendlovic, *Appl. Opt.* **34** (1995) 828.

3. L. Juarez, M. Cywiak, B. Barrientos, and J.M. Flores, *Opt. Commun.* **268** (2006) 209.

4. L. Juarez, M. Cywiak, M. Servín, and J.M. Flores, *Opt. Express* **15** (2007) 5277.

5. T. Kikukawa and H. Utsunomiya, *Microsc. Microanal.* **7** (2001) 363.

6. S. Kai, I. Chun, and D. Ping, *Opt. Express* **14** (2006) 4452.

7. M Yamaguchi *et al.*, *Jour. Microsc.* **194** (1998) 552.

8. T. Choi and T.D. Milster, *Opt. Eng.* **45** (2006) 64302.

9. J.H. Coombs and A.H.M. Holtslag, "*Scanning optical microscopy: a powerful tool in optical recording,*" in *Optical Data Storage '91*, J.J. Burke, T.A. Shull and N. Imamura, eds., *Proc. SPIE* **1499** (1991) 6.

10. T.E. Karis *et al.*, "*Verification of tracking servo signal simulation from scanning tunneling microscope surface profiles,*" in *Optical Data Storage '91*, J.J. Burke, T.A. Shull and N. Imamura, eds., *Proc. SPIE* **1499** (1991) 366.

11. B.A. Sexton and G.F. Cotterill, *J. Vac. Sci. Technol. A* **7**, (1989) 2734.

12. M. Mansuripur *et al.*, *App. Opt.* **35** (1997) 9296.

13. B. Wolfring, T. Weber, T. Mueller-Wirts and M. Mansuripur, "*Versatest-I, a versatile polychromatic dynamic testbed for optical disks,*" in *Recent Advances in Metrology, Characterization, and Standards for Optical Digital Data Disks*, F.L. Podio, eds., *Proc. SPIE* **3806** (1999) 2.

14. J. Butty, D. Kraehenbuehl, and B.J. Bartholomeusz, "*Methods for characterization of phase change optical discs,*" in *Recent Advances in Metrology, Characterization, and Standards for Optical Digital Data Disks*, F.L. Podio, eds., *Proc. SPIE* **3806** (1999) 76.

15. Y. Kashihara, *et al.*, "*Simulation study for high density optical disk systems,*" in *Optical Data Storage 2001*, T. Hurst and S. Kobayashi, eds., *Proc. SPIE* **4342** (2001) 524.

16. W. Ulf, "*Local track pitch measuring apparatus and method,*" US 2004/0081048 **A1** (2004) 1.

17. R. Köning *et al.*, "*Step height metrology for data storage applications,*" in *Recent Advances in Metrology, Characterization, and Standards for Optical Digital Data Disks*, F.L. Podio, eds., *Proc. SPIE* **3806** (1999) 21.

18. D.A. Chernoff, J.D. Lohr, D. Hansen, and M. Lines, "*High precision calibration of a scanning probe microscope (SPM) for pitch and overlay measurements,*" in *Metrology, Inspection, and Process Control for Microlithography XI*, S.K. Jones, eds., *Proc. SPIE* **3050** (1997) 243.

19. R.L. Wilkinson and J.H. Rilum, "*DVD Mastering using dye polymer media,*" in *Optical Data Storage '97*, H. Birecki and J. Z. Kwiecien, eds., *Proc. SPIE* **3109** (1997) 160.

20. C.S. Cook, D.A. Chernoff, and D.L. burkhead, "*Automated analysis of data mark microstructure of various media in the optical disc industry,*" in *Optical Data Storage 2000*, D.G. Stinson and R. Katayama, eds., *Proc. SPIE* **4090** (2000) 16.

21. D.L. Burkhead and D.A. Chernoff, "*AFM analysis of wobble amplitude,*" in *International Symposium on Optical Memory and Optical Data Storage Topical Meeting* (Institute of Electrical and Electronics Engineers, New York, 2002), pp. 359.

22. A. Kuhle, B.-G. Rosen, and J. Garnaes, "*Comparison of roughness measurement with atomic force microscopy and interference microscopy,*" *Proc. SPIE* **5188** (2003) 154.